Robustness of the Data-Driven Identification algorithm with altered input data

Marie Dalémat, Michel Coret, Adrien Leygue, Erwan Verron

Robustness of the Data-Driven Identification algorithm with altered input data

Marie Dalémat[†], Michel Coret[†], Adrien Leygue[*†], and Erwan Verron[†]

[†]Institut de Recherche en Génie Civil et Mécanique (GeM), UMR CNRS 6183, École Centrale de Nantes, France

January 25, 2021

Abstract

Identifying the mechanical response of a material without presupposing any constitutive equation is possible thanks to the Data-Driven Identification algorithm developed by Leygue *et. al.* (*Data-based derivation of material response*. Computer Methods in Applied Mechanics and Engineering **331**, 184–196 (2018)). This algorithm allows to measure stresses from displacement fields and forces applied to a given structure; the peculiarity of the technique is the absence of underlying constitutive equation. In the case of real experiments, the algorithm has been successfully applied in Dalémat *et. al.* (*Measuring stress field without constitutive equation*. Mechanics of Materials **136**, 103087 (2019)), where a perforated elastomer sheet is deformed under large strain. Displacements are gathered with Digital Image Correlation and net forces with a load cell. However, those real data are incomplete for two reasons: some displacement values (close to the edges or in a noise-affected area) are missing and the force information is incomplete with respect to the original DDI algorithm requirements. The present study proves that with appropriate data handling, stress fields can be identified in a robust manner. The solution relies on recovering those missing data smartly enough, so that no assumption, except that the application of the balance of linear momentum has to be made. The influence of input parameters of the method is also discussed. The overall study is conducted on synthetic data: perfect and altered data are used to prove robustness of the proposed solutions. Therefore, the paper can be considered as a practical guide for implementing the DDI method.

Keywords: Data Driven Identification, Digital Image Correlation, Altered data, Stress measurement

[*]Corresponding author: Adrien.Leygue@ec-nantes.fr

1 Introduction

Constitutive equations are historically essential in Mechanics of Materials to perform analytical or numerical calculations: they close the problem when combined with mechanical equilibrium. In practice, the identification procedure consists in choosing or deriving a constitutive model that describes well the material response. Then, the calibration of the model parameters has to be done ideally considering multiple deformation states (uniaxial tension, pure shear, biaxial tension...), which renders difficult the experimental process. These steps are often done iteratively to end up with a robust and well-calibrated constitutive model. With the evolution of full-field measurement techniques such as Digital Image Correlation [1], identification methods are constantly being improved, specifically with non-standards tests. For example, [2] and [3] gave an overview of identification techniques such as the Virtual Fields Method or the Finite Element Model Updating Method. Concomitantly, with the emergence of Data Sciences, other methods are proposed: for example, [4] and [5] trained a neural network for identification purposes.

Here, a new path is chosen: identifying the material response with no underlying constitutive equation. Indeed, it is possible to use the previous techniques (full-field methods and Data Sciences) to create rich databases that can be used for identification but also for simulation. It overcomes the difficulties in getting a robust identification of the model parameters. This has been introduced in [6] where the constitutive equations is replaced by a discrete database of strain-stress couples. The corresponding approach is referred to as Data-Driven Computational Mechanics (DDCM). Slightly different formulations of this solver are proposed in [7], [8], [9], [10] and several extensions are discussed in [11], [12], [13].

Concerning material characterization, non-parametric approaches are proposed by [14] and [15] in which the strain energy function of a hyperleastic material is not presupposed but computed with splines, thanks to experimental simple tests. In [16], a decomposition of the strain fields obtained with Digital Image Correlation is made in order to compute the stress field without constitutive equation. In [17], experimental dynamic measurements are used in the balance equations so that stress fields can be directly computed.

In the present paper, a specific algorithm called Data Driven Identification (DDI) is considered; it has been recently proposed in [18]. It allows to identify heterogeneous stress fields from measured displacement fields and external forces, without constitutive equation. It relies on the availability of heterogeneous and rich data which can be smartly clustered so that a strain-stress database is built without constitutive equations. It has been validated with synthetic data [18] and its application to real data has been recently assessed [19]. It is an innovative tool to measure stress fields, from DIC gathered displacement fields and net forces measured by load cells.

The difficulty in applying the DDI algorithm to real data lies mainly in the incompleteness and noisiness of data in some areas of the samples. Indeed, unlike a synthetic problem where everything is perfectly known, neither all forces nor all displacements can be perfectly measured; these difficulties are overcome by making **preprocessing choices** (both on the two intrinsic parameters of the algorithm and on the experimental input data). The so-called preprocessing step transforms raw input data to well-

conditioned input data with consistent parameters for the DDI algorithm. The present work demonstrates the robustness and the reliability of the DDI algorithm when applied to incomplete data: several possible preprocessing choices are compared so that the proper one can be applied with confidence.

The paper is organized as follow:

- A brief recall of the algorithm is proposed in order to highlight its optimal parameters and input data;
- Then, a case study is built to study several preprocessing choices. Synthetic data are considered for which the reference stress response is known. These synthetic data are modified to simulate incomplete data representative of reality;
- Then, a parametric study is conducted to find the proper preprocessing choice. It focuses on:
  (i) the **intrinsic parameters** (of the algorithm) when using the DDI with perfect data;
  (ii) the preprocessing step for **incomplete input data** (missing displacements and forces);
- Finally, the proper preprocessing choice is summarized so that the DDI method can be applied with confidence on real (*i.e.* partial and noisy) data. It gives the reader the possibility to implement him/herself the DDI method for real data.

2 Recall of the Data Driven Identification algorithm

This section is recalling the DDI algorithm so that its optimal parameters and input data are highlighted. The Data Driven Identification (DDI) [18] corresponds to the inverse method of Data Driven Computational Mechanics (DDCM) derived in [6]. This method identifies the complete response of a structure without using constitutive equation, from a large database.

2.1 Input data

We consider a 2D-meshed geometry, deformed over N_X increments indexed by X. For this geometry, the following data are the inputs of the algorithm and are considered to be available:

(I-1) the nodal displacements $\boldsymbol{u}_j^X$, j being the node number. The strain derived from the displacements is the Hencky's true strain tensor $\ln \boldsymbol{v}$. It is defined from $\boldsymbol{b}$, the left Cauchy-Green tensor, by:

$$\ln \boldsymbol{v} = \frac{1}{2} \ln \boldsymbol{b}, \tag{1}$$

with $\boldsymbol{b} = \boldsymbol{F}\boldsymbol{F}^T$, $\boldsymbol{F}$ being the deformation gradient tensor. In practice, a Digital Image Correlation software provides displacement fields on a grid. A mesh with associated connectivity is built from it to compute $\boldsymbol{F}$,

(I-2) the matrix $\boldsymbol{B}_{ej}^X$ which encodes geometry and connectivity, e being the quadrature point number. In particular, the mechanical balance can be evaluated at all nodes by:

$$\sum_e w_e^X \boldsymbol{B}_{ej}^X \cdot \boldsymbol{\sigma}_e^X = \boldsymbol{f}_j^X \quad \forall X, j, \tag{2}$$

where w_e^X is the integration weight of point e at loading step X,

(I-3) the nodal forces $\boldsymbol{f}_j^X$. These are zero in the absence of body forces, excepted for boundary nodes.

Additionally, the method has two intrinsic parameters:

(Inp-1) the size N^* of the (stress-strain) database that samples the material response,

(Inp-2) the positive definite tensor $\mathbb{C}$ that defines the distance between two points in the phase space (here, the stress-strain space).

2.2 Output of the method

After convergence of the algorithm, the N_X mechanical problems are solved and the method gives:

(O-1) the stress fields $\boldsymbol{\sigma}_e^X$ that satisfy the mechanical balance in each node j according to Eq. (2). The stress $\boldsymbol{\sigma}_e^X$ (calculated) and the strain $\ln \boldsymbol{v}_e^X$ (measured) are referred to as a *mechanical state*, as they are mechanically admissible (balanced and compatible),

(O-2) the N^* material states $(\ln \boldsymbol{v}_i^*, \boldsymbol{\sigma}_i^*)$, N^* being chosen by the user (Inp-1). These material states can be interpreted as a sampling of the material strain-stress response surface. Their distance from mechanical states is defined by an energetic norm $||\cdot||_{\mathbb{C}}^2$ defined in Eq. (3) where $\mathbb{C}$ is a fourth order positive definite tensor also chosen by the user (Inp-2).

2.3 Solver

The algorithm aims at finding material states that are as close as possible to statically and kinematically admissible mechanical states (the latter being half known: the strain field is known, the stress field not), according to the energetic norm $||\cdot||_{\mathbb{C}}^2$ defined by:

$$||(\ln \boldsymbol{v}, \boldsymbol{\sigma})||_{\mathbb{C}}^2 = \frac{1}{2}(\ln \boldsymbol{v} : \mathbb{C} : \ln \boldsymbol{v} + \boldsymbol{\sigma} : \mathbb{C}^{-1} : \boldsymbol{\sigma}). \tag{3}$$

The problem is formulated as follows:

$$\text{solution} = \arg \min_{\boldsymbol{\sigma}_e^X, (\ln \boldsymbol{v}_i^*, \boldsymbol{\sigma}_i^*)} \mathscr{E}(\boldsymbol{\sigma}_e^X, \ln \boldsymbol{v}_e^{*X}, \boldsymbol{\sigma}_e^{*X}), \tag{4}$$

with,

$$\mathscr{E}(\boldsymbol{\sigma}_e^X, \ln \boldsymbol{v}_e^{*X}, \boldsymbol{\sigma}_e^{*X}) = \sum_X \sum_e w_e^X ||(\ln \boldsymbol{v}_e{}^X - \ln \boldsymbol{v}_e^{*X}, \boldsymbol{\sigma}_e{}^X - \boldsymbol{\sigma}_e^{*X})||_{\mathbb{C}}^2, \tag{5}$$

and subject to the constraints

- of respecting the mechanical balance Eq. (2),
- that the material state $(\ln \boldsymbol{v}_e^{*X}, \boldsymbol{\sigma}_e^{*X})$ associated to the element e of increment X belongs to the database $(\ln \boldsymbol{v}_i^*, \boldsymbol{\sigma}_i^*)_{i=1}^{N^*}$.

Therefore, the DDI outputs are:

- the mechanical states,
- the database of material states,
- the mapping between mechanical and material states.

In the initial work [18], the validity of the method has been demonstrated with perfect synthetic data (from (I-1) to (I-4)). In the experimental validation [19], the algorithm has been applied with incomplete data that are well-preprocessed. The purpose of this paper is to carefully study the preprocessing choices to prove the reliability of the algorithm.

3 Building the case study

In this section, a case study is developed to study several preprocessing choices. First, features of usual real data are presented then several preprocessing options are proposed, with a focus on missing data. Finally, the methodology for the next section is summarized.

3.1 From idealized to realistic input data

Experimental data might have missing information and can be noisy. Here, the construction of the actual realistic problem from perfect synthetic data is explained thanks to a 2D example. Noise on the displacement field measurements has to be taken into account. The typical noise in DIC is considered to have an amplitude of the order of 1 pixel, independently of the measured displacement. The discussion of the effect of noisy displacement values is beyond the scope of this paper and has already been partially addressed in the original DDI publication [18].

3.1.1 Why are some data missing?

The DDI method is applied to a perforated hyperelastic membrane subjected to uniaxial tension. The mechanical problem and the different notations are provided in Figure 1a.

Synthetic data are altered according to usual experimental observations:

- we cannot measure the nodal forces but a net force,
- displacements are sometimes missing in areas called *clusters* (which are larger than just a few pixels): the latter are the DIC results when using a software that does not provide the considered unreliable displacements (due to large strain, noise or loss of speckles for example),

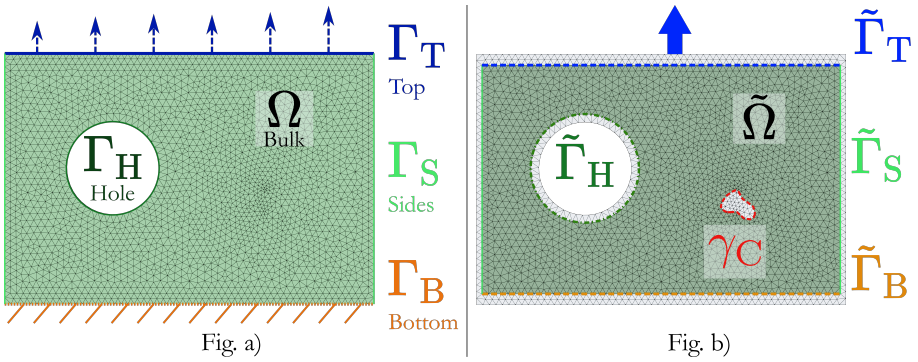

Figure 1: a) Theoretical problem b) Real problem with three particular modified boundaries: top boundary with grip, *cluster* of missing data and imperfectly defined edges close to hole.

- displacements are also missing close to edges: both the camera and the DIC software which works on a manually preselected region cannot resolve the edges of the part. In addition, most correlation software use rectangular patterns that cannot account for curved edges.

The mechanical problem with real boundaries is thus provided in Figure 1b.

In the figures, the theoretical boundaries are the top boundary (Γ_T) where the force is applied, the sides boundaries (Γ_S) that are free edges, the bottom boundary (Γ_B) which is clamped and the hole boundary which is free (Γ_H). In the real problem, all the boundaries are close but not exactly identical to the actual ones. They are noted $\tilde{\Gamma}_T$ for the top, $\tilde{\Gamma}_S$ for the sides, $\tilde{\Gamma}_B$ for the bottom and $\tilde{\Gamma}_H$ for the hole boundaries. Plus, the cluster of missing data is defined by its boundary denoted γ_C.

3.2 Possible preprocessing options for missing data

The preprocessing choices concern both the intrinsic parameters of the DDI method and the way of dealing with raw data. First, the preprocessing choices regarding the missing data are detailed.

With such experimental data, it is necessary to rewrite some equations of the initial DDI algorithm given in Section 2. Indeed, handling properly the areas where data are missing is fundamental to insure reliability. Several possibilities are proposed to deal with the missing data:

- In the area near the grip, where the force is measured (the "t" stands for the top boundary):

  (t-0) In the synthetic case, we know each nodal force $\boldsymbol{f}_j^X$ at the top boundary Γ_T;

  (t-1) Using a load cell, only the sum of the forces $\boldsymbol{f}_j^X$ on the top boundary Γ_T in the loading direction $\boldsymbol{n}_{\text{sol}}$ is known:

$$\sum_{j \in \Gamma_T} \boldsymbol{f}_j^X \cdot \boldsymbol{n}_{\text{sol}} = F_{\text{cell}}^X \quad \forall X. \tag{6}$$

It is thus possible to define a global equilibrium condition on the boundary, by combining Eqs. (2) and (6):

$$\sum_{j\in\Gamma_{\mathrm{T}}}\sum_{e} w_e^X \boldsymbol{B}_{ej}^X \cdot \boldsymbol{\sigma}_e^X \cdot \boldsymbol{n}_{\mathrm{sol}} = F_{\mathrm{cell}}^X \quad \forall X. \tag{7}$$

(t-2) In the real case, the displacements close to the grips are not measured and the true boundary cannot be considered in the algorithm. Thus, the boundary Γ_{T} cannot be considered and is replaced by $\tilde{\Gamma}_{\mathrm{T}}$. To deal with the force information, the simplest solution is to assume that Eq. (7) applies also on $\tilde{\Gamma}_{\mathrm{T}}$ as follow:

$$\sum_{j\in\tilde{\Gamma}_{\mathrm{T}}}\sum_{e} w_e^X \boldsymbol{B}_{ej}^X \cdot \boldsymbol{\sigma}_e^X \cdot \boldsymbol{n}_{\mathrm{sol}} = F_{\mathrm{cell}}^X \quad \forall X. \tag{8}$$

- For *clusters* of missing displacement values, the objective function Eq. (5) cannot be evaluated in some elements which should be removed from the problem along with associated nodes.

(c-1) A simple and naive solution is to simply discard the equilibrium constraint for these nodes.

(c-2) Another solution is to consider that the boundary of *clusters* is the boundary of a mechanically balanced subset. Indeed, a global balance condition is prescribed on the boundary γ_{C}. This is equivalent to consider a zero net force on this boundary. This can be easily explained by the Ostrogradsky-Gauss theorem in the continuous formulation:

$$\int_{\Omega_{\mathrm{C}}} \mathrm{div}\boldsymbol{\sigma}\mathrm{dV} = \int_{\gamma_{\mathrm{C}}} \boldsymbol{\sigma}\cdot\mathbf{n}\mathrm{dS} = \int_{\gamma_{\mathrm{C}}} \mathbf{f}\mathrm{dS}, \tag{9}$$

which gives, for the discrete formulation:

$$\sum_{j\in\gamma_{\mathrm{C}}}\sum_{e} w_e^X \boldsymbol{B}_{ej}^X \cdot \boldsymbol{\sigma}_e^X = \mathbf{0}. \tag{10}$$

- For edges close to holes, the perfect case is the one where the mesh boundary coincides with the real edge of the hole and the free edge condition applies. It is denoted (h-0) and will be the reference case (the "h" stands for the hole boundary). In the real case, due to the imperfect edge definition, the displacement values in the vicinity of holes edges are not known. Therefore, the data on the real boundary Γ_{H} are not known and $\tilde{\Gamma}_{\mathrm{H}}$ must be considered instead. On this boundary, several assumptions can be made:

(h-1) The free edge assumption can be adopted if we consider that $\tilde{\Gamma}_{\mathrm{H}}$ is really close to Γ_{H} so the edge is free. This incorrect assumption is likely to introduce a bias in the predictions.

(h-2) A weaker assumption consists in applying a zero net force on this boundary. It is verified as the missing matter should be mechanically balanced (like in (c-2)):

$$\sum_{j\in\tilde{\Gamma}_{\mathrm{H}}}\sum_{e} w_e^X \boldsymbol{B}_{ej}^X \cdot \boldsymbol{\sigma}_e^X = \mathbf{0}. \tag{11}$$

These strategies to deal with missing data are summarized in Figure 2.

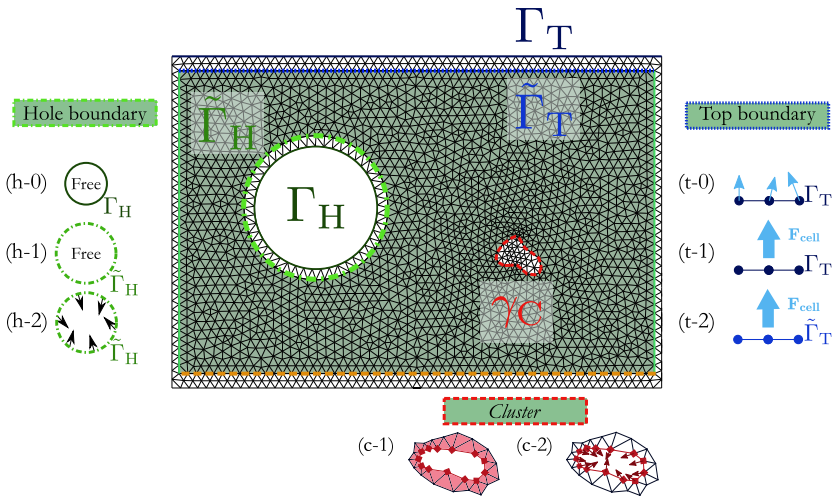

Figure 2: Summary of the preprocessing choices to analyze. They concern the missing data for three particular boundaries: top boundary with grip, *cluster* of missing data and imperfectly defined edges close to hole.

3.3 Methodology in practice

3.3.1 Inputs and parameters

The methodology to investigate the robustness of the DDI is to compare several cases of synthetic input data that are deteriorated on purpose. The cases are studied with respect to the intrinsic parameters of the DDI algorithm. As a recall, the inputs of the algorithm are:

- The algorithm parameters (intrinsic to the resolution method): N^* and $\mathbb{C}$,
- The measured data, especially displacements and forces, which might be incomplete.

Therefore, the discussion is organized as follows:

1. First, the effects of intrinsic parameters on a case where the input data are prefect are analyzed;
2. Second, the influence of the incomplete measured data is analyzed: the cases of (t-0), (t-1) and (t-2) related to the top grip are compared, the cases of (c-1) and (c-2) related to the *clusters* of missing data are discussed, and finally the cases of (h-0), (h-1) and (h-2) related to the edges close to the holes are considered.

3.3.2 Reference model

It is necessary to build synthetic data for which the reference response is known. Thus, a standard Finite Element model (made with the software Abaqus™) is used. The

Coefficient	Value	Units
μ_1	$6.18 \cdot 10^5$	[Pa]
μ_2	$1.18 \cdot 10^3$	[Pa]
μ_3	$-9.81 \cdot 10^3$	[Pa]
α_1	1.3	[−]
α_2	5.0	[−]
α_3	−2.0	[−]

Table 1: Ogden parameters to build the reference solution [20].

geometry is given in Figure 3 where the initial and deformed meshes of the problem are presented. The initial height is denoted h_0.

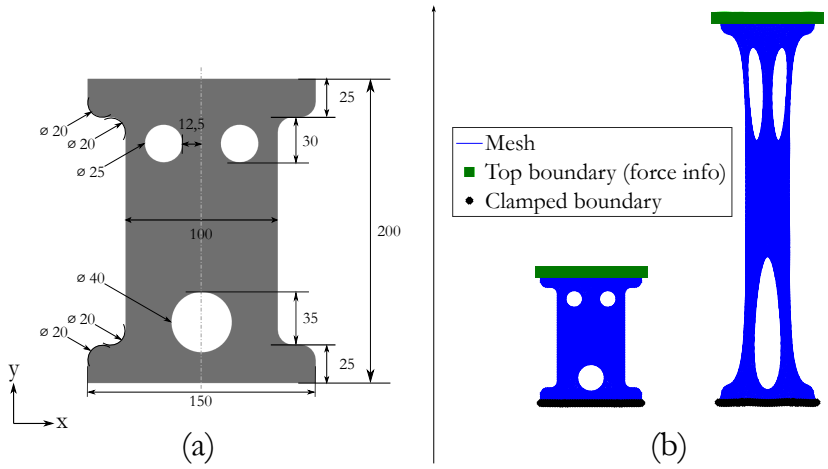

Figure 3: Case of study: a perforated hyperelastic membrane under uniaxial tension ((a): initial mesh; (b) : after 200% of total macroscopic strain). On the top nodes, information on force is available while the bottom ones are clamped.

The Ogden model [20] is chosen and the equation describing the strain energy density is:

$$W(\lambda_1, \lambda_2, \lambda_3) = \sum_{i=1}^{n} \frac{\mu_i}{\alpha_i} \left(\lambda_1^{\alpha_i} + \lambda_2^{\alpha_i} + \lambda_3^{\alpha_i} - 3 \right). \tag{12}$$

The values of the parameters are given in Table 3.3.2. They are identified in [20] to fit experimental data in [21].

$N_e = 6108$ linear triangular finite elements under plane stress condition are chosen. The displacements are prescribed using a (x, y) coordinate system corresponding to the horizontal and vertical directions, respectively. They are given for the top and bottom

boundaries (denoted Γ_{T} and Γ_{B}) by:

$$\begin{cases} u_x = 0 \quad \text{on} \quad \Gamma_{\mathrm{T}} \\ u_y = 2h_0 \quad \text{on} \quad \Gamma_{\mathrm{T}} \\ u_x = 0 \quad \text{on} \quad \Gamma_{\mathrm{B}} \\ u_y = 0 \quad \text{on} \quad \Gamma_{\mathrm{B}}. \end{cases} \tag{13}$$

The finite element computation is decomposed into $N_X = 21$ increments under quasi-static loading conditions. It gives the reference stresses in each element denoted $\boldsymbol{\sigma}_{\mathrm{FE}}$. The strain fields, meshes and loading conditions are used as inputs in the DDI algorithm with the preprocessing choices introduced in the previous section, resulting in an identified stress field, denoted $\boldsymbol{\sigma}_{\mathrm{DDI}}$.

3.3.3 Error in stress identification

As the purpose of the DDI is to measure stress field without constitutive equation, the global error between the stress field identified by the DDI $\boldsymbol{\sigma}_{\mathrm{DDI}}$ and the reference one $\boldsymbol{\sigma}_{\mathrm{FE}}$ is computed for all loading increments X and all elements e by:

$$\mathrm{e} = \frac{\sum\limits_{X,e} ||\boldsymbol{\sigma}_{\mathrm{FE},e^X} - \boldsymbol{\sigma}_{\mathrm{DDI},e^X}||_2}{\sum\limits_{X,e} ||\boldsymbol{\sigma}_{\mathrm{FE},e^X}||_2}. \tag{14}$$

4 Results and discussion

This section presents the results which consist in comparing several altered cases. The aim is to determine the proper preprocessing choices that ensure robustness and reliability for stress identification. The influence of the intrinsic parameters of the DDI algorithm is first discussed with perfect input data. Then, the incompleteness of input data and the preprocessing choices associated are discussed.

4.1 Influence of intrinsic parameters

The number of material states N^* is the parameter that allows to sample more or less finely the response of the material. It is to be compared to the total number of degrees of freedom of the problem: $N_e \times N_X = 128\ 268$. We define the sampling ratio $r^* = (N_e \times N_X)/N^*$ and consider that it varies between 2 and 10^4.

The distance to mechanical states $(\ln \mathbf{v}_e^X, \boldsymbol{\sigma}_e^X)$ is defined by the energetic norm $||\cdot||^2_{\mathbb{C}}$ of Eq. (3). The simplest form for the tensor $\mathbb{C}$ is spherical with an amplitude C:

$$\mathbb{C} = C\mathbb{I}, \tag{15}$$

where $\mathbb{I}$ is the fourth-order identity tensor. This form aims to equally weight all components of the strain and stress fields. C is defined accordingly to a pseudo-tangent elasticity modulus of the behavior model used in finite element analyses: $C_0 = 2.3 \cdot 10^6$ Pa. It is computed by the slope of the straight line found by the least mean square

method in the $(||\ln \mathbf{v}||_{\mathrm{VM}}, ||\boldsymbol{\sigma}||_{\mathrm{VM}})$ space (von Mises norm). Practically, we choose values of C ranging from C_0 to $10^6 C_0$.

Figure 4 shows the identification error, after convergence. The left subfigure presents

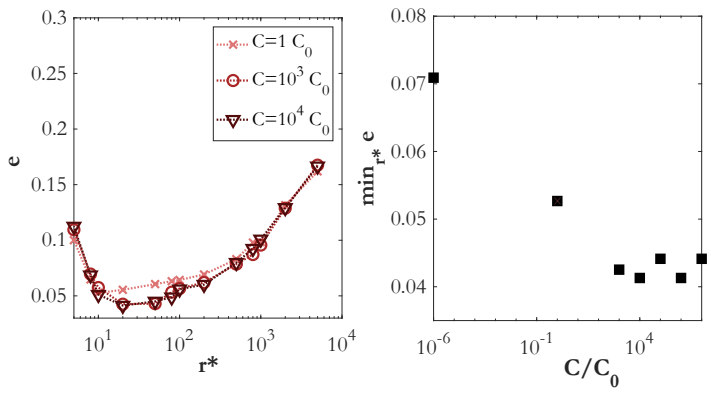

Figure 4: Influence of the intrinsic parameters N^* (related to r^*) and C without missing data. The error is compared to r^* (left subfigure), and the minimum error is compared to C (right subfigure).

the error as a function of the sampling ratio r^* for different values of C. For each C value, the minimum error (with respect to r^*) is reported. Then, the minimum error (for the optimal value of r^*) in relation to C/C_0 is shown in the right subfigure. The error is minimal for $r^* \approx 20$ (10 to 50 depending on the C value). A large ratio (not enough material states) implies a sub-sampling of the response and therefore a significant error. Conversely, a too small ratio (too many material states) produces an effect comparable to *overfitting* in regression: the behavior is no longer averaged sufficiently, which also leads to a significant error. It is therefore necessary to choose a value between these two extremes; these results are similar to those obtained in [18].

In addition, C significantly contributes to the convergence of the method: the higher it is (to a certain extent), the lower the error is. Indeed, the distance defined by the norm influences the mapping between material and mechanical states. By choosing a large value of C, the mapping based on strain values is favored, which is relevant since they are measured (and so reliable) unlike stresses which evolve during the convergence of the algorithm. Finally, N^* is more influential than C: without missing data, a bad choice of N^* will never be compensated by a good choice of C.

4.2 Influence of the incompleteness of input data

4.2.1 Force input

First, we consider preprocessing choices related to force information: either with all nodal forces (t-0), or represented by their net value on the true boundary (t-1) or the net force on the approximate boundary (t-2). The influence of N^* on the error is reported

in Figure 5 (for $C = 10^3 C_0$). Global errors are similar: a sampling ratio r^* from 20 to

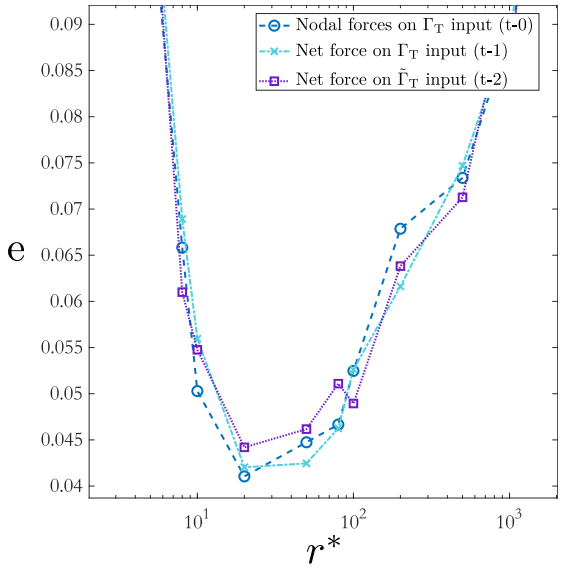

Figure 5: Influence of force inputs on the error as a function of r^* for (t-0) the given nodal forces, and (t-1) and (t-2) the given net force on respectively the true boundary and the approximate boundary.

100 is preferable. It shows that the DDI results are only slightly influenced by the way these equilibrium conditions are prescribed on the top boundary.

For a local insight, Figure 6 presents the nodal forces computed with the stress identified with the DDI in case (t-1). They are compared to the reference ones (case (t-0)). They are really similar which means that stresses computed with the DDI are almost as perfect as the reference ones, even if the input in force is the net force only.

4.2.2 *Cluster* of missing data

We consider the influence of the preprocessing choices related to a *cluster*: by handling it naively (c-1) and in a mechanically optimal way (c-2). The influences of r^* and C on the error are shown in Figure 7.

In the case of a naively handled *cluster* (c-1), it is difficult to achieve a small error. Too many or too few material states lead to more important errors. Here, the choice of C is crucial: the larger it is (within a certain limit), the closer we get to a mapping based on strains (which are known). By simply adding the zero net force condition (c-2) on the boundary, as proposed in Eq. (10), a robustness similar to results without missing data is recovered. In this case, the choice of C is much less critical than that of N^*.

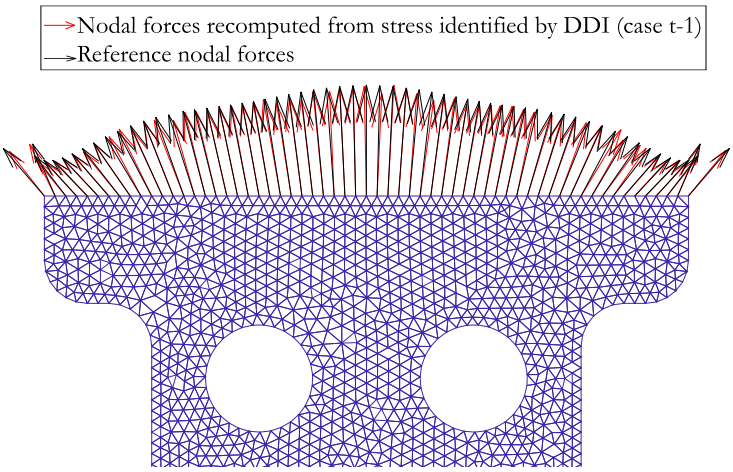

Figure 6: Nodal forces computed with the identified stress for the case (t-1) compared to the reference nodal forces (t-0).

4.2.3 Imperfect resolution close to holes

Finally, we consider the influence of the preprocessing choices in the case of an imperfect resolution close to the edges, on the boundary $\tilde{\Gamma}_{\mathrm{H}}$. The case of (h-1) the free edge assumption on this boundary and the case of (h-2) zero net force over the boundary $\tilde{\Gamma}_{\mathrm{H}}$ are compared to the perfect case with no missing data close to the edge (h-0). Errors are plotted for a given C with respect to the sampling ratio r^* in Figure 8.

Considering the free edge assumption leads to a large error, whereas the globally balanced assumption again induces a small error, close to the ideal case. Then, it is interesting to study the stress distribution as one approaches the hole: the von Mises stress is plotted along a line of the sample for the three cases, as depicted in Figure 9. For the free edge assumption (h-0), the algorithm predicts a misplaced stress increase close to the wrongly presumed free edge. Stresses are overestimated around the hole and this overestimation propagates to the bulk by equilibrium relations which are global. Therefore, the best manner to handle an imperfect edge consists in adopting a mechanically correct assumption: only a zero net force condition must be enforced. In this case (h-2), the error is similar to the one with no missing data. The optimal ratio r^* is again between 20 and 100.

4.2.4 Summary

To close this discussion on how to handle properly incomplete input data, Figure 10 presents the three stress components identified considering the corrections depicted in the left-hand side subfigure. The incomplete input data have to be completed smartly with only the mechanical balance equation: (t-2),(c-2),(h-2). It leads to results similar to the perfect case: the global error is less than 0.05.

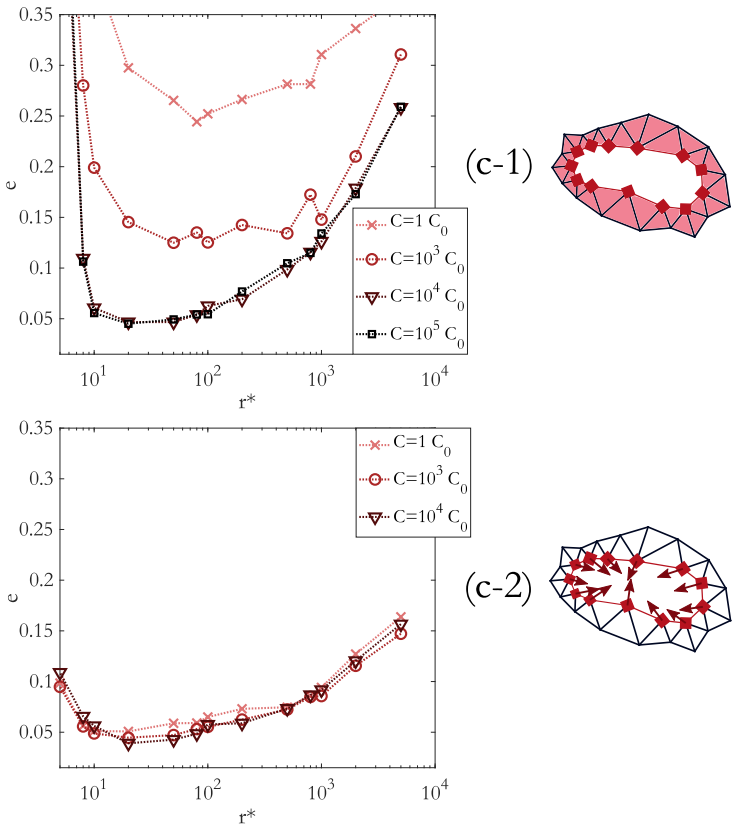

Figure 7: Influence of the preprocessing choice with a *cluster* on the error as a function of r^* and C for cases (upper subfigure) (c-1) naive and (lower subfigure) (c-2) mechanically optimal

The preprocessing choices that bring the best robustness when dealing with missing data are summarized in Figure 11. These are the choices made in the experimental validation [19] of the DDI algorithm.

5 Closure: implementation of the DDI with real data

In this work, the input parameters of the DDI algorithm have been examined, with the objective of identifying correctly the stress field without constitutive equation. A study of its intrinsic parameters confirms our previous work. In particular, the consequences of incomplete data (inherent to experimental data) is analyzed through two aspects: the availability of net forces instead of nodal forces on the computational mesh, and

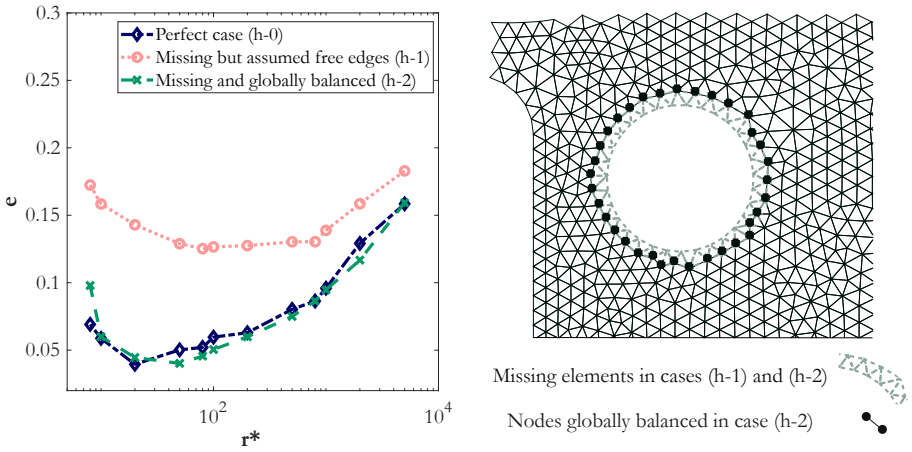

Figure 8: Influence of preprocessing choice for the hole edge definition on the error as a function of r^* for a given C, for the cases of an imperfectly defined edge close to the hole (with (h-1) the assumption of free edge, (h-2) the global balance condition) and of a perfectly defined edge (h-0) (left subfigure). Nodes/elements used in the calculations (right subfigure).

the difference between the actual part geometry and the computational mesh. This last aspect appears either through *clusters* of missing data (areas of a few pixels/elements) and the imperfect edge definitions close to holes and boundaries. We demonstrate that the robustness of the method is ensured when incomplete data are managed under a strict mechanical point of view.

To conclude, we propose to adapt the original DDI algorithm to real experimental data. The boundaries defined in Figure 1 are considered. The solution of the problem is still defined as:

$$\text{solution} = \arg \min_{\boldsymbol{\sigma}_e^X, (\ln \boldsymbol{v}_i^*, \boldsymbol{\sigma}_i^*)} \mathscr{E}(\boldsymbol{\sigma}_e^X, \ln \boldsymbol{v}_e^*, \boldsymbol{\sigma}_e^*), \tag{16}$$

with $\mathscr{E}$ defined in Eq. (5), and subject to the (new) constraints:

- respecting the mechanical balance equations:
  - locally:
$$\sum_e w_e^X \mathbf{B}_{ej}^X \cdot \boldsymbol{\sigma}_e^X = \mathbf{0} \quad \forall X, \forall j \in \tilde{\Omega} \cup \tilde{\Gamma}_{\mathrm{B}}, \tag{17}$$
  - globally:
$$\sum_{j \in \Delta^X} \sum_e w_e^X \mathbf{B}_{ej}^X \cdot \boldsymbol{\sigma}_e^X = \mathbf{F}_{\Delta^X} \quad \forall X, \tag{18}$$
    with Δ^X representing each boundary on which is applied the net force $\mathbf{F}_{\Delta^X}$, at the increment X *i.e.*:

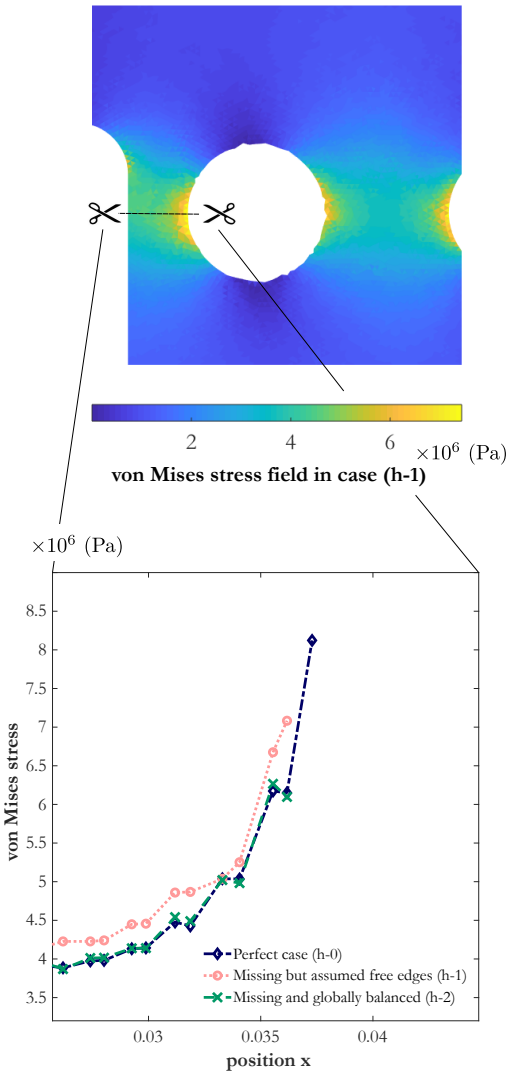

Figure 9: von Mises stress field (lower subfigure) and reported values along a horizontal line going through the sample (upper subfigure), for the three cases.

- ∗ the top boundary $\tilde{\Gamma}^X_{\mathrm{T}}$ on which the net force is the one measured by the load cell $F^X_{\mathrm{cell}}\boldsymbol{n}_{\mathrm{sol}}$;
- ∗ the boundary around *clusters* of missing data γ^X_{C} on which a zero net force is applied;
- ∗ the boundary around a hole $\tilde{\Gamma}^X_{\mathrm{H}}$ on which a zero net force is applied;

• ensuring that the material state $(\ln \boldsymbol{v}^*_{e^X}, \boldsymbol{\sigma}^*_{e^X})$ associated to the element e^X belongs

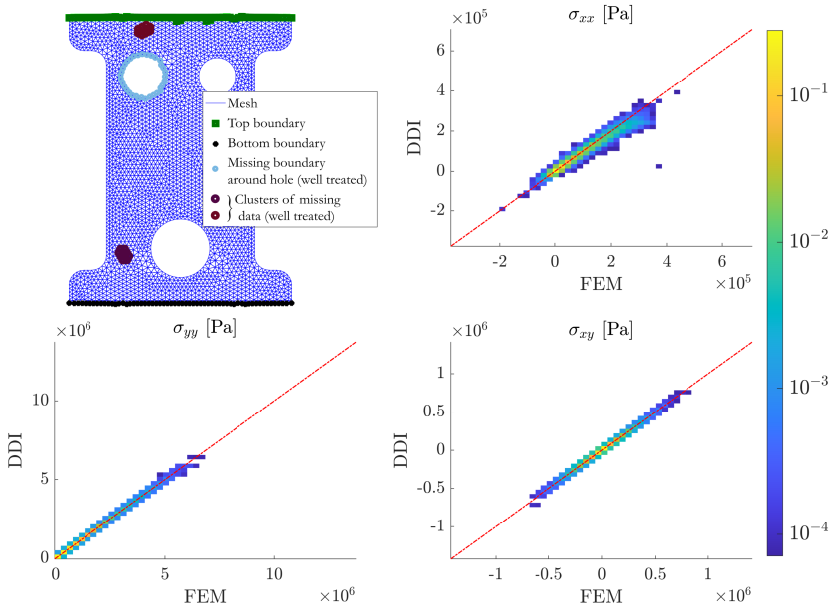

Figure 10: Comparison between reference stress fields and identified stress fields with DDI for a geometry with the proper preprocessing choices for missing data. The colors in the 2D histograms represent the histogram bin probability for each stress component.

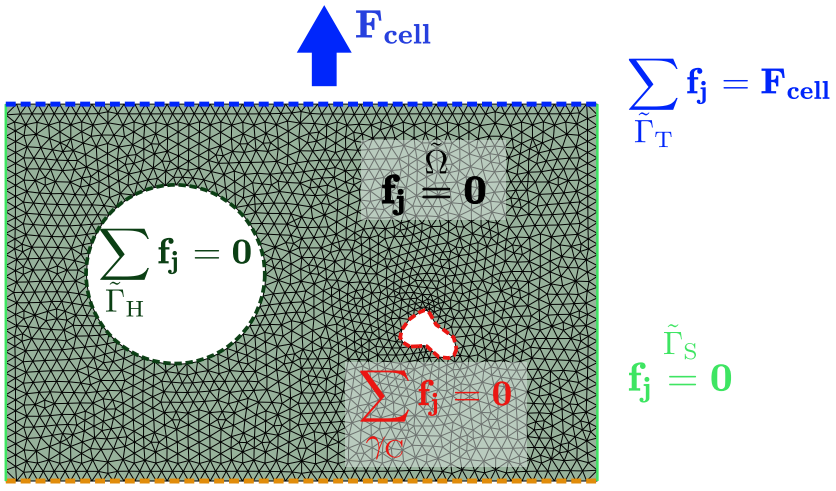

Figure 11: Summary of the proper preprocessing choice to deal with three particular boundaries (top boundary with a global force information, *cluster* of missing data and imperfectly defined edges close to a hole).

to the database $(\ln \boldsymbol{v}_i^*, \boldsymbol{\sigma}_i^*)_{i=1}^{N^*}$.

The implementation details can be found in the original paper [18]. For the intrinsic parameters, it is advised to choose N^* so that the sampling ratio r^* is 100 and to choose $\mathbb{C} = C\mathbb{I}$ with $C \geqslant 10^3 C_0$, C_0 being the average stiffness of the material and $\mathbb{I}$ the fourth-order identity tensor.

Acknowledgements: This work was performed by using HPC resources of Centrale Nantes Supercomputing Center on the cluster Liger, granted and identified D1705030 by the High Performance Computing Institute (ICI).

References

[1] M. A. Sutton, J. J. Orteu, H. Schreier, Image Correlation for Shape, Motion and Deformation Measurements: Basic Concepts,Theory and Applications, Springer Science & Business Media, 2009.

[2] S. Avril, M. Bonnet, A.-S. Bretelle, M. Grédiac, F. Hild, P. Ienny, F. Latourte, D. Lemosse, S. Pagano, E. Pagnacco, F. Pierron, Overview of identification methods of mechanical parameters based on full-field measurements, Experimental Mechanics 48 (4) (2008) 381. doi:10.1007/s11340-008-9148-y.
URL https://link.springer.com/article/10.1007/s11340-008-9148-y

[3] S. Roux, F. Hild, Optimal procedure for the identification of constitutive parameters from experimentally measured displacement fields, International Journal of Solids and Structures In Press, Corrected Proof (DOI : 10.1016/j.ijsolstr.2018.11.008) (Nov. 2018). doi:10.1016/j.ijsolstr.2018.11.008.
URL http://www.sciencedirect.com/science/article/pii/S0020768318304542

[4] T. Furukawa, G. Yagawa, Implicit constitutive modelling for viscoplasticity using neural networks, Numerical Methods in Engineering 43 (1998) 195–219.

[5] H. Yang, X. Guo, S. Tang, W. K. Liu, Derivation of heterogeneous material laws via data-driven principal component expansions, Computational Mechanics 64 (2) (2019) 365–379. doi:10.1007/s00466-019-01728-w.
URL https://doi.org/10.1007/s00466-019-01728-w

[6] T. Kirchdoerfer, M. Ortiz, Data-driven computational mechanics, Computer Methods in Applied Mechanics and Engineering 304 (2016) 81–101. doi:10.1016/j.cma.2016.02.001.
URL http://www.sciencedirect.com/science/article/pii/S0045782516300238

[7] J. Ayensa-Jiménez, M. H. Doweidar, J. A. Sanz-Herrera, M. Doblaré, A new reliability-based data-driven approach for noisy experimental data with physical constraints, Computer Methods in Applied Mechanics and Engineering 328 (2018) 752–774. doi:10.1016/j.cma.2017.08.027.
URL http://www.sciencedirect.com/science/article/pii/S0045782517304255

[8] Y. Kanno, Simple Heuristic for Data-Driven Computational Elasticity with Material Data Involving Noise and Outliers: A Local Robust Regression Approach, arXiv:1708.05794 [math] (Aug. 2017).
URL http://arxiv.org/abs/1708.05794

[9] T. Kirchdoerfer, M. Ortiz, Data Driven Computing with noisy material data sets, Computer Methods in Applied Mechanics and Engineering 326 (2017) 622–641. doi:10.1016/j.cma.2017.07.039.
URL http://www.sciencedirect.com/science/article/pii/S0045782517304012

[10] L. T. K. Nguyen, M.-A. Keip, A data-driven approach to nonlinear elasticity, Computers & Structures 194 (2018) 97–115. doi:10.1016/j.compstruc.2017.07.031.
URL http://www.sciencedirect.com/science/article/pii/S0045794917301311

[11] T. Kirchdoerfer, M. Ortiz, Data-driven computing in dynamics, International Journal for Numerical Methods in Engineering 113 (11) (2018) 1697–1710. doi:10.1002/nme.5716.

[12] S. Conti, S. Müller, M. Ortiz, Data-Driven Problems in Elasticity, Archive for Rational Mechanics and Analysis 229 (1) (2018) 79–123. doi:10.1007/s00205-017-1214-0.
URL https://doi.org/10.1007/s00205-017-1214-0

[13] R. Eggersmann, T. Kirchdoerfer, S. Reese, L. Stainier, M. Ortiz, Model-Free Data-Driven inelasticity, Computer Methods in Applied Mechanics and Engineering 350 (2019) 81–99. doi:10.1016/j.cma.2019.02.016.
URL http://www.sciencedirect.com/science/article/pii/S0045782519300878

[14] M. Latorre, F. J. Montáns, Experimental data reduction for hyperelasticity, Computers & Structures In Press, Corrected Proof (DOI : 10.1016/j.compstruc.2018.02.011) (Mar. 2018). doi:10.1016/j.compstruc.2018.02.011.
URL http://www.sciencedirect.com/science/article/pii/S0045794917306259

[15] J. Crespo, F. J. Montáns, General solution procedures to compute the stored energy density of conservative solids directly from experimental data, International Journal of Engineering Science 141 (2019) 16–34.

doi:10.1016/j.ijengsci.2019.05.013.
URL http://www.sciencedirect.com/science/article/pii/S0020722517327635

[16] J. Réthoré, A. Leygue, M. Coret, L. Stainier, E. Verron, Computational measurements of stress fields from digital images, International Journal for Numerical Methods in Engineering 113 (12) (2018) 1810–1826. doi:10.1002/nme.5721.
URL https://onlinelibrary.wiley.com/doi/abs/10.1002/nme.5721

[17] R. Seghir, F. Pierron, A Novel Image-based Ultrasonic Test to Map Material Mechanical Properties at High Strain-rates, Experimental Mechanics 58 (2) (2018) 183–206. doi:10.1007/s11340-017-0329-4.
URL https://doi.org/10.1007/s11340-017-0329-4

[18] A. Leygue, M. Coret, J. Réthoré, L. Stainier, E. Verron, Data-based derivation of material response, Computer Methods in Applied Mechanics and Engineering 331 (2018) 184–196. doi:10.1016/j.cma.2017.11.013.
URL http://www.sciencedirect.com/science/article/pii/S0045782517307156

[19] M. Dalémat, M. Coret, A. Leygue, E. Verron, Measuring stress field without constitutive equation, Mechanics of Materials 136 (2019) 103087.

[20] R. W. Ogden, Large deformation isotropic elasticity: on the correlation of theory and experiment for compressible rubberlike solids, Proc. R. Soc. Lond. A 328 (1575) (1972) 567–583. doi:10.1098/rspa.1972.0096.
URL http://rspa.royalsocietypublishing.org/content/328/1575/567

[21] L. R. G. Treloar, Stress-strain data for vulcanised rubber under various types of deformation, Transactions of the Faraday Society 40 (0) (1944) 59–70. doi:10.1039/TF9444000059.
URL http://pubs.rsc.org/en/content/articlelanding/1944/tf/tf9444000059